Geophysical Research Letters

RESEARCH LETTER
10.1029/2022GL100262

Key Points:

- A submesoscale frontal slick is documented in a lake for the first time; it evolved on the warm side of a surface temperature front
- The temperature front was formed by mesoscale circulation that separated relatively warm surface water from colder upwelling-induced water
- The slick was 10-km long and its width increased by a factor of four in 1.5 hr due to "feeding" by wind-driven small-scale slicks

Supporting Information:

Supporting Information may be found in the online version of this article.

Correspondence to:

M. Foroughan,
mehrshad.foroughan@epfl.ch

Citation:

Foroughan, M., Hamze-Ziabari, S. M., Lemmin, U., & Barry, D. A. (2022). A persistent submesoscale frontal slick: A novel marker of the mesoscale flow field in a large lake (Lake Geneva). *Geophysical Research Letters*, *49*, e2022GL100262. https://doi.org/10.1029/2022GL100262

Received 7 JUL 2022
Accepted 13 OCT 2022

A Persistent Submesoscale Frontal Slick: A Novel Marker of the Mesoscale Flow Field in a Large Lake (Lake Geneva)

Mehrshad Foroughan[1], Seyed Mahmood Hamze-Ziabari[1], Ulrich Lemmin[1], and David Andrew Barry[1]

[1]Ecological Engineering Laboratory (ECOL), Faculty of Architecture, Environmental Engineering Institute (IIE), Civil and Environmental Engineering (ENAC), Ecole Polytechnique Fédérale de Lausanne (EPFL), Lausanne, Switzerland

Abstract Submesoscale fronts often become visible when the accumulation of biosurfactants in the water surface microlayer causes smooth surfaces, called frontal slicks, to develop. Based on in situ and remotely-sensed data, a frontal slick was documented for the first time in a lake (Lake Geneva). A quasi-stationary ~10-km long slick formed on the warm side of a surface temperature front with strong horizontal velocity strain. The slick width increased from ~50 to ~200 m in ~1.5 hr due to "feeding" by wind-driven, rapidly-moving smaller slicks. Numerical modeling results, confirmed by satellite data, indicated that the boundary between mesoscale gyres isolated warm surface water from cold water associated with wind-induced coastal upwelling. Measurements and modeling suggest that frontogenetic sharpening of the submesoscale temperature gradient created an active front with strong convergent flow. Such dynamics must be considered in buoyant material transport and the vertical exchange of surface water with deeper layers in lakes.

Plain Language Summary Near-surface currents in lakes are affected by interactions of structures of different scales, such as gyres, eddies and coastal upwelling. These interactions can lead to the formation of fronts that are zones of convergence and downwelling, leaving floating materials to concentrate on the surface. Fronts are important because they can modify the lateral transport of surface material and the exchange between near-surface and deeper layers. Among the floating materials, biosurfactants create smooth surface areas (slicks) by suppressing capillary gravity waves, thus allowing visual detection of fronts in remote imaging. This study, carried out in Lake Geneva, documents for the first time the existence of a submesoscale (~10 km) frontal slick in a lake. Three-dimensional numerical modeling and satellite imagery showed that due to the interaction of mesoscale gyres and eddies with coastal upwelling, a thermal front was generated in the area where the frontal slick was observed. In situ field measurements provided evidence that the observed slick was located on the warm side of the predicted thermal front. Since frontal slicks are easy to observe and track, they can provide valuable information about mesoscale dynamics in lakes, which at present are poorly understood.

1. Introduction

In oceans, submesoscale motions (horizontal scales 0.1–10 km; McWilliams, 2016) can cause convergence and have significant vertical velocities within structures such as fronts when surface divergence, δ, and vertical vorticity, ζ, have larger magnitudes than the Coriolis frequency, f, that is, $|\delta/f| \geq 1$ and $|\zeta/f| \geq 1$ (Mahadevan & Tandon, 2006). Fronts are elongated in one direction and have a narrow width (McWilliams, 2021). In coastal waters, oceanic fronts were observed in regions with prominent upwelling or along the edges of high-discharge river plumes (Akan et al., 2018; Garvine, 1974; O'Donnell et al., 1998; Wang et al., 2021). They can also develop within strongly sheared currents in the open ocean, where mesoscale straining sharpens preexisting density gradients, also referred to as frontogenesis (Gula et al., 2014; McWilliams, 2021). Although their significance in the transport of energy and material in oceans is recognized (Choi et al., 2020; McWilliams, 2016), front studies in lakes are rare, and are mainly limited to thermal bars observed in the nearshore zone during spring and fall (Fichot et al., 2019; Naumenko et al., 2012).

Density fronts are typically associated with strong convergence that leads to the accumulation of surface material (e.g., D'Asaro et al., 2018). As a result, fronts can be observed as bands of materials floating on the surface, sometimes exhibiting distinct wave-field characteristics (Rascle et al., 2017, 2020) in response to wave-current interactions (Kudryavtsev et al., 2005; Phillips, 1984). Surface roughness can also vary near frontal convergence zones due to the accumulation of biogenic surfactants, usually under low wind conditions (<6 m s^{-1}). Accumulation of natural surfactants, typically derived from biological processes (Kujawinski et al., 2002; Kurata et al., 2016; Ẑutić et al., 1981), create relatively smooth surfaces known as slicks by damping short Gravity-Capillary Waves (GCW) (Watson et al., 1997).

Slicks can therefore reveal underlying flow structures, such as density fronts in satellite or airborne optical and radar images (Font et al., 2002; Karimova, 2012). Marmorino et al. (2002) explored frontal dynamics by observing slick evolution. Ryan et al. (2010) studied recurring slicks linked to a surface temperature front. Despite their relevance to near-surface hydrodynamics, frontal slicks in lakes have yet to be investigated.

In order to gain insight into frontal slick dynamics in a lake, we investigated a frontal slick that extended across a considerable portion of the width of Lake Geneva. Measurements indicate that the slick was associated with a Lake Surface Water Temperature (LSWT) submesoscale front. The measurements were complemented by three-dimensional (3D) numerical modeling of the lake hydrodynamics that showed how the front developed. Satellite imagery of LSWT confirmed the presence of the simulated front. The following questions are addressed:

- How does the frontal slick evolve in relation to the frontal dynamics?
- What causes the LSWT gradients and submesoscale currents responsible for the observed front formation and sharpening?
- What are the spatiotemporal variations in temperature and currents in the near-surface layer (down to ∼1.5 m depth) across the front?

The Supporting Information S1 provides details on certain aspects discussed in the manuscript with figures and texts prefixed S.

2. Materials and Methods

2.1. Study Site

Lake Geneva (*Lac Léman*) is a warm oligomictic lake located between Switzerland and France at a mean altitude of 372 m. It is Western Europe's largest lake with a length of 70 km, a maximum width of 14 km, a surface area of 582 km^2, a volume of 89 km^3, and a maximum depth of 309 m. The surrounding mountainous topography guides the wind field, resulting in two dominant strong winds coming from the northeast and southwest called the *Bise* and *Vent*, respectively (Lemmin & D'Adamo, 1996).

2.2. Measurement Methods

In situ field and remote data were collected using the following equipment and methods:

- An mobile two-platform measurement system (Figure S1, Text S1 in Supporting Information S1; Barry et al., 2019; Rahaghi et al., 2019) composed of:
  a) A 7-m long autonomous catamaran called ZiviCat that measured near-surface water temperatures (down to 1.5 m), near-surface currents (0.5–1 m depth), and wind speed and direction. Two forward-facing red-green-blue (RGB) cameras recorded images of surface water roughness. All ZiviCat data could be visualized in real time on the accompanying boat (*Elodea*).
  b) A 9-m^3 balloon called BLIMP at ∼400 m height, tethered to the boat, carried an imaging package that recorded RGB and infrared (IR) images (Figure 3a) to examine the spatial variability of the LSWT. Images could be visualized in real time on the boat (Liardon & Barry, 2017).
- Smooth patches and the rippled water around the frontal slick were sampled to determine surfactant concentrations. Water samples were collected using the glass-plate method for the uppermost 20–150 μm of the surface (Cunliffe et al., 2013) and hand-dipping to collect bulk water (20 cm below the surface) following standard procedures (Cunliffe & Wurl, 2014). The water sample analysis is described in Text S2 in Supporting Information S1.
- A shore-based imaging system, called TLB, installed 192 m above the lake surface on the lake's steeply rising northern shore, took (angled-view) RGB images that allowed surface slick detection across most of the lake's width (for location, see Figure 1a). Images can be visualized in real time on the boat and the tilt and pan angles of the camera can be remotely controlled from the boat.

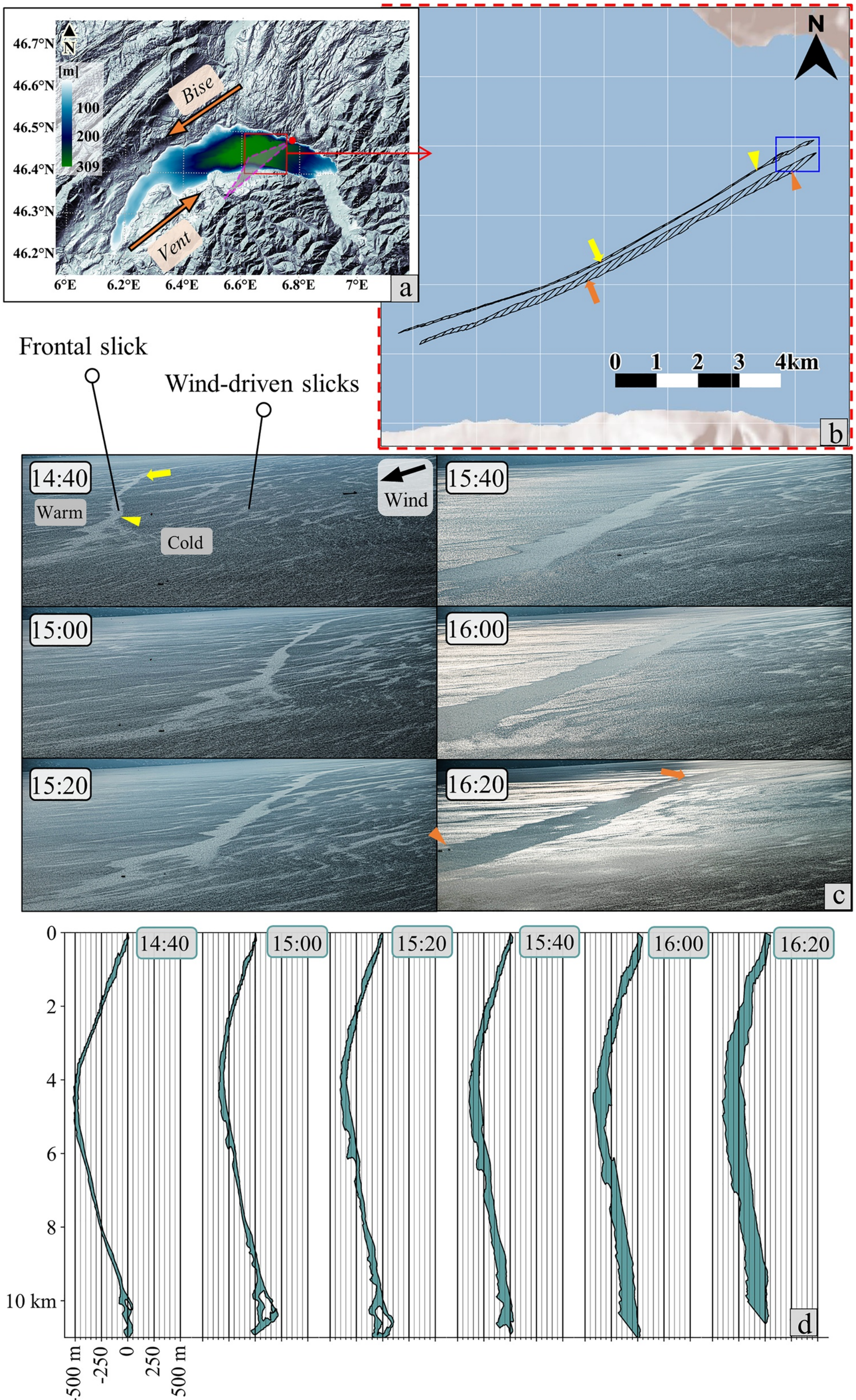
46.7°N
46.6°N
46.5°N
46.4°N
46.3°N
46.2°N
N
[m]
100
200
309
Bise
Vent
6°E
6.2°E
6.4°E
6.6°E
6.8°E
7°E
a
N
0 1 2 3 4km
b
Frontal slick
Wind-driven slicks
14:40
Warm
Cold
Wind
15:40
15:00
16:00
15:20
16:20
c
14:40
15:00
15:20
15:40
16:00
16:20
0
2
4
6
8
10 km
-500 m
-250
0
250
500 m
d

Figure 1.

- Advanced Very High Resolution Radiometer (AVHRR) satellite data with a 1-km grid resolution was used to obtain whole-lake LSWT images (Riffler et al., 2015).

All the above was combined with 3D numerical modeling of Lake Geneva, based on the validated model setup of Cimatoribus et al. (2018), which provided details of the lake hydrodynamics during the field measurement campaign (Text S3 in Supporting Information S1).

3. Results

The field campaign was carried out on Lake Geneva on 30 September 2020, during the summer stratification season with a thermocline at ∼20–30 m depth. Observations were made between 14:00 and 16:30 (local time) when a ∼10 km long, slow-moving frontal slick evolved (Figure 1c). The wind was from the west and wind speed varied between 3 and 5 m s^{-1} (Figure 3a).

3.1. Frontal Slick Evolution

Images taken with the remote TLB camera are dominated by a long narrow slick with a sharp edge on the western (upwind) side extending across most of the width of the lake basin (Figure 1c). Over a period of 1.5 hr, the slick changed little in shape, was only slightly displaced and did not change its orientation suggesting a frontal slick. This was further confirmed by comparing its position in the first and last images (Figure 1b). The frontal slick forms to the east of a sharp temperature gradient (Figure 3).

Geo-rectified snapshots of the frontal slick (Figure 1d) showed that it had a large aspect ratio that decreased over time (Figure 1e), that is, it widened almost four-fold (from ∼50 to ∼200 m) during 1.5 hr while moving very slowly eastward. (Figures 1e and 3c and Movie S1). The rapid movement of smaller slicks with the wind (∼3 m s^{-1}, Figure 1d) suggests that wind-driven drift currents drive their kinematics, whereas the frontal slick maintained a large angle with the wind. The slow eastward movement of the frontal slick indicated that its motion was predominantly controlled by underlying lake hydrodynamics.

Slicks in the images have smooth surfaces that are caused by the accumulation of surfactants. To verify that surfactant concentrations are different in the observed smooth frontal slick and the rough-surface surrounding areas, 10 water samples were collected around the northern tip of the frontal slick (Figure 1c) between 14:45 and 15:20. Higher enrichment of Fluorescent Dissolved Organic Matter, a proxy for natural surfactants (Frew et al., 2002; Salter, 2010), was found inside the frontal slick (Text S2, Figure S2 in Supporting Information S1) whose smooth surface suppressed GCW formation as confirmed by images simultaneously taken by the ZiviCat RGB camera (Movie S2).

3.2. Mesoscale and Submesoscale Flow Structures Leading to Front Formation

During the 6 days preceding the campaign, strong *Vent* wind events from the southwest with wind speeds up to 10 m s^{-1} prevailed over the lake (Figures S2a–S2c in Supporting Information S1). They produced a set of rotational flow patterns seen in the results of the high-resolution 3D modeling (Figure 2b) and caused coastal upwelling along the northern shore. On 30 September, two Anticyclonic Gyres (AG1 and AG2; clockwise rotating) and the two Cyclonic Eddies (CE1 and CE2; counterclockwise) formed in the eastern and central parts of the lake (Figure 2b), and a thermal front had developed between AG1 and AG2. Good agreement is found between the large-scale modeled LSWT and that in the satellite image for the same time; both indicate a horizontal LSWT difference between the western and the eastern parts of the lake, separated by a sharp front at about the same location (Figures 3a and 3b), thus confirming the validity of the modeling results. The lateral displacement between the front location seen in the measurements (Figure 1) and in the satellite image and the

Figure 1. (a) Lake Geneva's bathymetry and the surrounding mountainous topography, Red dot: location of on-shore camera TLB. Magenta triangle: field of view of the TLB camera. *Bise* and *Vent* are the two dominant, strong large-scale winds blowing over most of Lake Geneva. (b) Map showing the georeferenced outlines of the first and last frontal slick images in (c). Blue rectangle: northern end of the slick where the in situ measurements (Figure 3) were taken. (c) Six TLB camera snapshots show the time evolution of the frontal slick. The approximate wind direction, two types of slicks, and the cold/warm side of the front are indicated in the first image. At 14:50, the camera was turned 5° to the east to follow the slick. The northern tip of the slowly moving slick left the field of view in later images. Locations of yellow and orange symbols correspond to those in (b) for reference. (d) Geo-rectified (Gerum et al., 2019) outlines of the frontal slick for the images in panel (c), illustrating its expansion over time. The water depth below the slick is always >100 m.

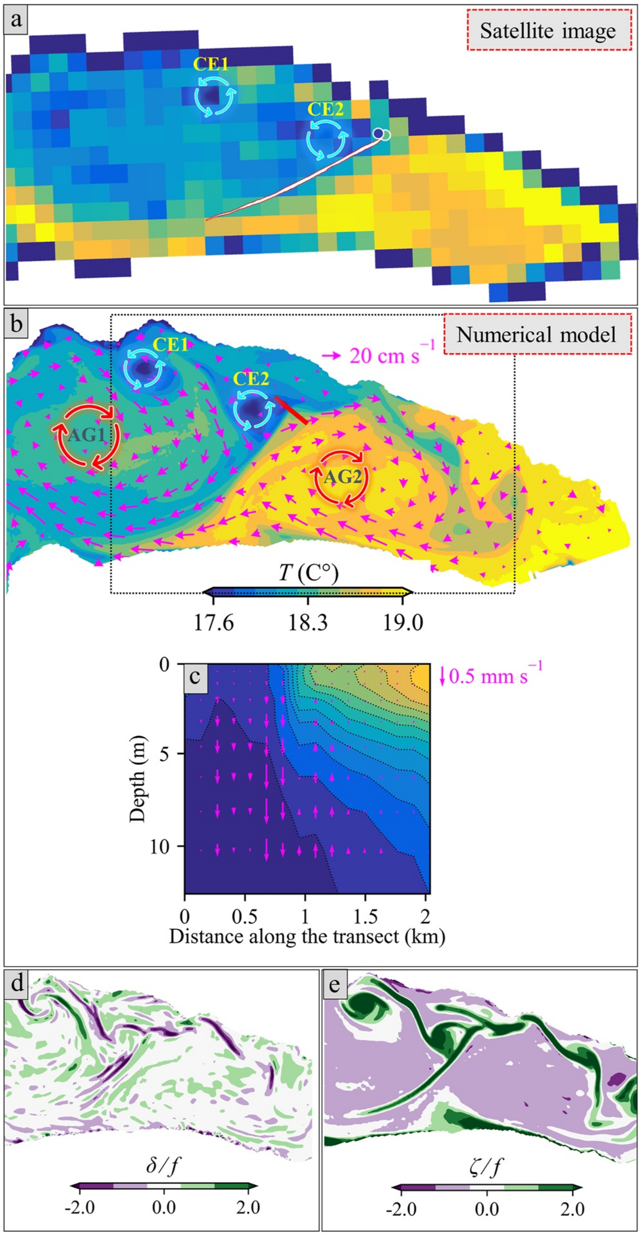

Figure 2. (a) Lake Surface Water Temperature derived from the Advanced Very High Resolution Radiometer satellite data (1 km grid cells) at 17:00 on 30 September 2020. Nearshore grid cells have lower temperatures since they also cover some surrounding land. Superimposed on the map is the frontal slick outline (Figure 1b) at 16:00 (white), along with two samples of in situ temperature measurements (at 5 cm depth) taken on both sides of the front (Figure 3b). (b) Snapshot of numerical simulation results at 16:00, 30 September 2020 of lake surface temperature with magenta arrows indicating currents. Gyres (AG1, AG2) and eddies (CE1, CE2) are highlighted with rotating arrows. The black dotted-lined rectangle marks the section of the lake displayed in (d and e). Colorbar: temperature range corresponding to panels (a–c). (c) Temperature and vertical velocity in a vertical plane along the red transect in (b). (d) horizontal divergence ($\delta = \partial u/\partial x + \partial v/\partial y$), and (e) vertical vorticity ($\zeta = \partial v/\partial x - \partial u/\partial y$) normalized by the Coriolis frequency (f), derived from the simulated surface currents.

simulated LSWT front may be due to limitations in the atmospheric forcing model (Text S3 in Supporting Information S1) and the selected drag coefficient (Rascle et al., 2020).

The high-resolution simulation permitted identification of submesoscale processes. Filamentary structures are evident in the instantaneous field of horizontal divergence, δ, and vertical vorticity, ζ (Figures 2a–2d). Their high normalized values in the frontal region suggest that submesoscale processes were well developed (McWilliams, 2017). Previous submesoscale-resolving models (Shcherbina et al., 2013) showed fronts and vortices emerging in regions with strong cyclonic vorticity similar to the vorticity field in Figure 2e. The strong convergence in Figure 2d indicates compensating downward motion of the denser water (Figure 2c), which can lead to frontogenic sharpening of the background LSWT gradient. Strong current gradients along the lake's northern shore may suggest slick formation; however, no remote observations are available for further analysis. Even though the model was run in hydrostatic mode, the results of temperature and velocity fields in the vertical direction (Figure 2c) offer, at least qualitatively, insight into the 3D flow structure of the front. Mahadevan and Tandon (2006) had pointed out that vertical velocities in a submesoscale front can be $\mathcal{O}$ (1 mm s^{-1}), which is also seen in the present results.

3.3. Surface and Near-Surface Cross-Front Variability

The frontal slick (Figure 1) and the thermal front (Figure 2) occur in the same area of the lake. To determine whether a relationship exists between the two, in situ measurements were carried out with the catamaran ZiviCat and the BLIMP balloon. The ZiviCat traversed the northern end of the LSWT front between ~15:29 and ~16:29 at five locations (Figures 3c and 3d, Movie S2), following a zigzag trajectory. The orientation of the tracks was selected based on monitoring of the frontal slick as seen in the TLB images, in the RGB images taken by the camera mounted on the front of the ZiviCat, and by the sharp temperature gradient in the remote BLIMP IR images (Figure 3a). All these data were available in real time on the boat accompanying the ZiviCat. During this period, the wind was blowing eastward toward the frontal slick (Figure 3a), as is evident from the motion of small slicks (Movie S1). In situ near-surface temperature measurements (Figure 3c), IR images obtained with the BLIMP package (Figure 3a), and pictures taken by the ZiviCat's onboard camera (Movie S2) confirm that the west (upwind) side of the slick coincides with the sharpest horizontal temperature gradient (0.7°C in ~10 m), that is, the LSWT and surface roughness were simultaneously modified in the cross-front direction over a relatively short distance. The smooth surface on the warm side of the front was only $\mathcal{O}$ (100 m) long (Figure 3c).

Although a sharp LSWT gradient is evident from the BLIMP images (Figure 3a, Movie S2) and from the topmost thermistors, the two bottom thermistors recorded a more gradual change, that is, a longer transition distance of $\mathcal{O}$ (100 m) (Figure 3c). This cross-front difference between the surface and 1.5-m temperature variations suggest a downward penetration of cold surface water in the front, as also seen in the numerical simulation results (Figure 2c). However, with distance from the transition zone in the front, temperature profiles on both sides indicate well-mixed conditions in the upper 1.5 m of surface water (Figures 3b and 3c).

The measured near-surface currents also revealed abrupt changes across the front (Figure 3a). The high-resolution Acoustic Doppler Current Profiler

10.1029/2022GL100262

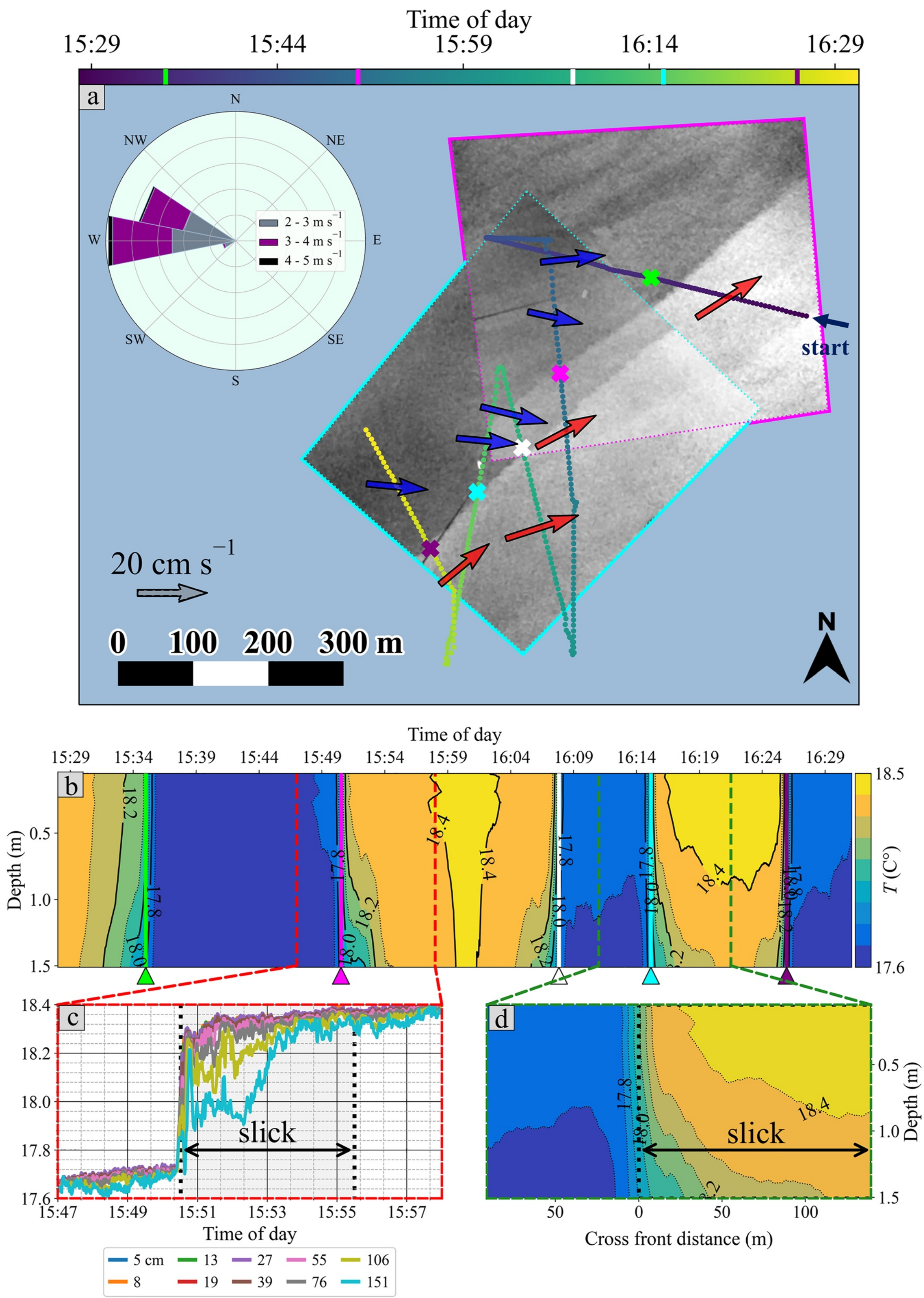

Figure 3.

(ADCP) measurements (depth-averaged from ∼0.5 to ∼1 m) were corrected for phase-wrapping effects and ZiviCat movement. On the cold western side of the LSWT front, currents were almost aligned with the wind direction (Figure 3a) and were nearly perpendicular to the front. Currents on the warm side, however, were directed to the northeast, forming an angle with the wind, consistent with anticyclonic circulation on the eastern side of the front in the model results (Figure 2b).

Current gradients in the cross-front direction were estimated as:

$$\frac{\partial \mathcal{V}}{\partial x} \approx \frac{\Delta \mathcal{V}}{\Delta x} = \frac{\overline{\mathcal{V}}_{10\mathrm{m,warm}} - \overline{\mathcal{V}}_{10\mathrm{m,cold}}}{10\mathrm{m}} \tag{1}$$

where x is in the cross-front direction and $\overline{\mathcal{V}}_{10\mathrm{m}}$ are the depth-averaged cross-front or along-front velocity components, averaged within a 10-m wide horizontal slice in the cross-front direction. Assuming that along- and cross-front velocities only vary in the cross-front direction (Garvine, 1974; Rascle et al., 2020; Figure 3a), both the horizontal divergence, δ, and vertical vorticity, ζ, can be derived from the current gradients as $\partial \mathcal{V}|_{\mathrm{cross-front}}/\partial x$ and $\partial \mathcal{V}|_{\mathrm{along-front}}/\partial x$, respectively. The mean convergence and vorticity based on the first four transects and normalized by the Coriolis frequency, f, were calculated as 52 ± 25 for horizontal divergence, δ, and 56 ± 29 for vertical vorticity, ζ. These values are an order of magnitude higher than those simulated, which have much lower spatial resolution (Figures 2d and 2e). However, they are comparable to the values reported by Rascle et al. (2020) near the front. The intense convergence ($\sim 5.5\mathrm{cms}^{-1}$ variation over 10 m) is similar to the widening rate of the frontal slick evolution ($150\mathrm{mh}^{-1} \cong 4.2\mathrm{cms}^{-1}$), although no link between these rates is evident.

4. Discussion

4.1. Development of the Frontal Slick

A combination of in situ and remotely sensed observations provided a comprehensive picture of a frontal slick development in Lake Geneva (sketch in Figure S1 in Supporting Information S1). The surface micro-layer water samples showed that the smooth band on the warm side of the LSWT front had higher concentrations of surfactants (Figure S2 in Supporting Information S1), emphasizing the role of natural surfactants in manifesting frontal dynamics by inhibiting GCW development, as confirmed in the RGB images taken by the ZiviCat when crossing the frontal slick (Movie S2). A previous study in Lake Geneva showed that smooth slicks are associated with biogenic surfactants (Foroughan et al., 2022) and that they suppress GCW development.

The multiscale appearance of slicks on the lake surface water (Figure 1c, Movie S1) indicates that different processes affect the surfactant distribution and revealed two distinct types of slicks: (a) a large persistent frontal slick (manifesting a density front) that hardly changed location (Figure 3a), and (b) numerous smaller slicks that continually changed shape, and rapidly moved in the direction of the wind. The small slicks appear to originate from relatively distant locations; thus, the frontal slick can collect materials coming from a wide surface area.

Also noteworthy is the asymmetric edge morphology and distribution of smooth areas between the upwind (cold) and downwind (warm) sides of the frontal slick. The edge on the upwind (western) side of the front is relatively uniform and smooth, whereas on the downwind eastern side, there are protrusions and occasionally some small elongated slicks "escape." Such waveform edge patterns resemble an instability mechanism previously observed during the disintegration of large slicks (Marmorino et al., 2008). However, the present frontal slick is in the

Figure 3. (a) Enlargement of the blue square in Figure 1b showing: (i) ZiviCat tracks from ∼15:29 to ∼16:29 (crosses indicate locations where the ZiviCat traversed the Lake Surface Water Temperature front), (ii) two partially overlapping BLIMP infrared (IR) grayscale images (darker indicates colder) showing the front, with a slight eastward drift (∼3 cm s^{-1}) between them. Top left (time: 15:50): cold western side of the front (dark gray); bottom right (time: 16:15): warm eastern side of the front (light gray), (iii) depth-averaged (0.5–1 m) horizontal Acoustic Doppler Current Profiler velocities on the warm eastern side (red arrows) and the cold western side (blue arrows) of the front (velocity scale given by the gray arrow), and (iv) 1 hr mean-wind speed and direction measured by the ZiviCat meteostation. Colorbar on top of panel (a): time along the ZiviCat track. Colors of the BLIMP image frames (magenta and cyan) correspond to those of the crosses of frontal crossing. (b) One-minute moving average temperature pattern in the top 1.5 m of the water along the ZiviCat zigzag trajectory shown in panel (a), repeatedly traversing the front as marked by triangles (colors correspond to crosses in (a)) at the bottom of the panel. (c) Detailed time series of the ten near-surface thermistors during the second crossing of the front, marked by red vertical dashed lines in (b) corresponding to a cross-front distance of ∼100 m. The extent of the frontal slick on the lake surface during this transect is indicated by two vertical black dashed lines. Thermistor depths are given in the legend. (d) Detailed cross-front temperature variation (fourth crossing), marked by green vertical dashed lines in (b) with the same temperature range.

integration phase, that is, the input of small slicks to the front is significantly greater than the output (Figure 1d). Frontal slick width evolution appears to be controlled primarily by these dynamics.

Numerical modeling shows that the thermal front and, consequently, the frontal slick, is characterized by a strong vertical velocity (Figure 2c), as was also reported by Mahadevan and Tandon (2006). This downwelling explains the sharp western edge of the frontal slick. ZiviCat observations indicate that the mean horizontal velocity orientation changes significantly across the front (Figure 3a). The near-surface current field on the cold western side is nearly aligned with the wind, whereas the warm eastern side of the front is more oriented along the direction of the front (Figure 3a); this may slow down the transport of surfactants leaving the front on the eastern side.

4.2. LSWT Front Formation and Sharpening

Although the observed frontal slick appears to have a time scale of hours (this slick was not present in the TLB images of the previous/following day), model results suggest that *Vent* episodes over the preceding 6 days primarily triggered the basin-scale events that contributed to the front formation. Previous studies demonstrated that *Vent* events generate gyres in the central part of Lake Geneva (Cimatoribus et al., 2019; Razmi et al., 2018), and that Ekman-type coastal upwelling occurred along the lake's northern shoreline during winter (Reiss et al., 2020). Although our observations were made in a different season/stratification, a similar process was observed in the simulation results (Figures S3d and S3e in Supporting Information S1). Cold waters upwelled along the northern shore and were advected by strong near-surface currents of the central AG1 (Figure S2g in Supporting Information S1), eventually forming a cold pool of water in the west and middle of the lake (Figure S2f in Supporting Information S1). The time-integrated effect of the *Vent*-induced upwelling and vertical mixing with deeper, colder water, combined with strong currents circulating local cold surface water, led to an intense LSWT drop for the whole lake (Figure S3 in Supporting Information S1). However, the boundary between the two AGs isolated warmer surface waters in the east, from the colder waters in the west, thereby forming the LSWT front (Figure 2b), with high normalized convergence and vorticity in the frontal region (Figures 2d and 2e). This is confirmed by the satellite image (Figure 2a). Cold water captured by CE2 further intensified the temperature gradient along the upper section of the front (Figure 2a and 2b, Figure S2f in Supporting Information S1). Oceanic fronts have also been observed along the edges of mesoscale eddies (McWilliams, 2021).

Such a horizontal basin-scale density gradient and an intense deformation flow associated with mesoscale circulations resulted in a strong submesoscale front. Frontogenesis, that is, sharpening of horizontal density gradients, occurs through surface convergence and downwelling on the cold side of the front. The numerical simulation results, consistent with the in situ measurements, illustrate large lateral temperature and velocity gradients, cyclonic vorticity and convergence, all suggesting that the observed front is at the stage of accelerated frontal sharpening. The simulated vertical velocity in the cross-front plane is indirect evidence of cold-water downward penetration at the front as indicated by the isotherm pattern (Figure 2c). Our in situ measurements confirmed that the cold water sinks below the warm water at the front (Figure 3d).

Submesoscale fronts usually last for a few hours or days, can be sharpened exponentially fast, remain active for a relatively short period (McWilliams, 2021), and eventually become inactive and turn into "fossil" structures (Rascle et al., 2020). The present observations show that the upwind edge location of the frontal slick is determined by the active, sharp LSWT front (Figure 3, Movie S2), in contrast to previous studies (Marmorino et al., 2002; Ryan et al., 2010).

The processes leading to the observed frontal dynamics and the frontal slick formation can be summarized as follows (Figure S1 in Supporting Information S1): A thermal front was produced by the interaction of rotational flow patterns that resulted from strong wind forcing during the days preceding the measurement campaign. It separates warm-water regions from cold-water regions (Figure 2). The cold water approaches the front from the northwest, slightly clockwise from the wind as expected for an Ekman layer (Figure 3a). When it reaches the front, it sinks beneath the warm water (Figures 2c and 3d). At the same time, small slicks transporting surfactants are driven by the wind toward the front (Figure 1). When these slicks reach the front, the buoyant surfactants cannot sink with the cold water. Instead, they cross over the front and are deposited at its southern edge forming a frontal slick along the length of the front (Figures 1 and 3c). With time, more and more of the small slicks feed into the frontal slick, thereby increasing the amount of accumulated surfactant and as a result, the frontal slick south of the thermal front widens in the nearly calm warm waters (Figure 1).

From long-term records of our shore-based imagery system TLB, filamentary slicks with spatial scales comparable to the one in the current study occur frequently and have a life span of hours. Such similarity in time scales may further emphasize the role of submesoscale dynamics in frontal slick formation which in turn can affect the dispersion of surface materials in the lake. In addition, TLB long-term records indicate that the location and the orientation of submesoscale slicks in the widest part of the lake change; this reflects the dynamics of the underlying gyre pattern (Cimatoribus et al., 2019). A frontal slick such as the one observed here can be classified as part of a broader category of submesoscale currents commonly observed in oceanic surface waters and recently in Lake Geneva (Hamze-Ziabari, Foroughan, et al., 2022; Hamze-Ziabari, Razmi, et al., 2022).

5. Summary and Conclusions

Field observations carried out in Lake Geneva documented for the first time the existence of a persistent submesoscale frontal slick in a lake. It was ∼10-km-long and evolved along the warm side of a surface temperature front. Numerical simulation results show that the background temperature gradient generated by time-integrated wind-induced upwelling and barrier-forming confluent currents due to mesoscale circulation result in a LSWT front in the lake. This was confirmed by satellite data. Cross-front in situ measurements: (a) support simulation results, (b) point to the submesoscale character of the observed front, possibly sharpened frontogenically by strong convergent motions, and (c) confirm that the frontal slick is the surface marker of the LSWT front. The results demonstrate the effectiveness of a submesoscale current pattern in accumulating surface materials and promoting slick formation. Long-term records of our remote imagery package indicate that submesoscale slicks are a ubiquitous feature on Lake Geneva, and are likely to occur on similar-sized lakes under comparable conditions. Such frontal slicks and their underlying processes represent a novel transport mode for surface material, including pollutants, and their downward transfer in lakes, and therefore should be considered in the development of effective lake management concepts.

Data Availability Statement

The in situ and remotely-sensed data and model results supporting the findings of this study are available online at https://doi.org/10.5281/zenodo.7199358.

Acknowledgments
This work was supported by the Swiss National Science Foundation (SNSF, Grant 178866). We thank Florian Breider (Central Environmental Laboratory, EPFL) for making available the Fluorescence Spectrometer and for his guidance in the laboratory analysis. We also thank the EPFL Limnology Center for providing meteorological data from the LéXPLORE platform. The support of our colleagues, specifically Htet Kyi Wynn and Benjamin Daniel Graf, in fieldwork and technical assistance is greatly appreciated. We would like to thank the reviewers for their constructive comments and suggestions.

References

Ẑutić, V., Ćosović, B., Marčenko, E., Bihari, N., & Kršinić, F. (1981). Surfactant production by marine phytoplankton. *Marine Chemistry*, *10*(6), 505–520. https://doi.org/10.1016/0304-4203(81)90004-9

Akan, Ç., McWilliams, J. C., Moghimi, S., & Özkan-Haller, H. T. (2018). Frontal dynamics at the edge of the Columbia River plume. *Ocean Modelling*, *122*, 1–12. https://doi.org/10.1016/j.ocemod.2017.12.001

Barry, D. A., Liardon, J.-L., Paccaud, P., Klaus, P., Shaik, N., Rahaghi, A. I., et al. (2019). A low-cost, autonomous mobile platform for limnological investigations, supported by high-resolution mesoscale airborne imagery. *PLoS One*, *14*(2), e0210562. https://doi.org/10.1371/journal.pone.0210562

Choi, J., Troy, C., Hawley, N., McCormick, M., & Wells, M. (2020). Lateral dispersion of dye and drifters in the center of a very large lake. *Limnology & Oceanography*, *65*(2), 336–348. https://doi.org/10.1002/lno.11302

Cimatoribus, A. A., Lemmin, U., & Barry, D. A. (2019). Tracking Lagrangian transport in lake Geneva: A 3D numerical modeling investigation. *Limnology & Oceanography*, *64*(3), 1252–1269. https://doi.org/10.1002/lno.11111

Cimatoribus, A. A., Lemmin, U., Bouffard, D., & Barry, D. A. (2018). Nonlinear dynamics of the nearshore boundary layer of a large lake (Lake Geneva). *Journal of Geophysical Research: Oceans*, *123*(2), 1016–1031. https://doi.org/10.1002/2017JC013531

Cunliffe, M., Engel, A., Frka, S., Gašparović, B. Ž., Guitart, C., Murrell, J. C., et al. (2013). Sea surface microlayers: A unified physicochemical and biological perspective of the air-ocean interface. *Progress in Oceanography*, *109*, 104–116. https://doi.org/10.1016/j.pocean.2012.08.004

Cunliffe, M., & Wurl, O. (2014). *Guide to best practices to study the ocean's surface*. Marine Biological Association of the United Kingdom for SCOR. Retrieved from http://www.scor-int.org/Publications/SCOR_GuideSeaSurface_2014.pdf

D'Asaro, E. A., Shcherbina, A. Y., Klymak, J. M., Molemaker, J., Novelli, G., Guigand, C. M., et al. (2018). Ocean convergence and the dispersion of flotsam. *Proceedings of the National Academy of Sciences of the United States of America*, *115*(6), 1162–1167. https://doi.org/10.1073/pnas.1718453115

Fichot, C. G., Matsumoto, K., Holt, B., Gierach, M. M., & Tokos, K. S. (2019). Assessing change in the overturning behavior of the Laurentian Great Lakes using remotely sensed lake surface water temperatures. *Remote Sensing of Environment*, *235*, 111427. https://doi.org/10.1016/j.rse.2019.111427

Font, J., Rousseau, S., Shirasago, B., García-Górriz, E., & Haney, R. L. (2002). Mesoscale variability in the Alboran Sea: Synthetic aperture radar imaging of frontal eddies. *Journal of Geophysical Research*, *107*(C6), 3059. https://doi.org/10.1029/2001JC000835

Foroughan, M., Lemmin, U., & Barry, D. A. (2022). Effects of natural surfactants on the spatial variability of surface water temperature under intermittent light winds on Lake Geneva. *Journal of Limnology*, *81*(1), 2048. https://doi.org/10.4081/jlimnol.2022.2048

Frew, N. M., Nelson, R. K., McGillis, W. R., Edson, J. B., Bock, E. J., & Hara, T. (2002). Spatial variations in surface microlayer surfactants and their role in modulating air-sea exchange. In *Gas transfer at water surfaces* In M. A. Donelan, W. M. Drennan, E. S. Saltzman, & R. Wanninkhof (Eds.) (Vol. 127, pp. 153–159). American Geophysical Union (AGU). https://doi.org/10.1029/GM127p0153

Garvine, R. W. (1974). Dynamics of small-scale oceanic fronts. *Journal of Physical Oceanography*, *4*(4), 557–569. https://doi.org/10.1175/1520-0485(1974)004<0557:DOSSOF>2.0.CO;2

Gerum, R. C., Richter, S., Winterl, A., Mark, C., Fabry, B., Le Bohec, C., & Zitterbart, D. P. (2019). CameraTransform: A Python package for perspective corrections and image mapping. *SoftwareX*, *10*, 100333. https://doi.org/10.1016/j.softx.2019.100333

Gula, J., Molemaker, M. J., & McWilliams, J. C. (2014). Submesoscale cold filaments in the Gulf stream. *Journal of Physical Oceanography*, *44*(10), 2617–2643. https://doi.org/10.1175/JPO-D-14-0029.1

Hamze-Ziabari, S. M., Foroughan, M., Lemmin, U., & Barry, D. A. (2022). Monitoring mesoscale to submesoscale processes in large lakes with Sentinel-1 SAR imagery: The Case of Lake Geneva. *Remote Sensing*, *14*(19), 4967. https://doi.org/10.3390/rs14194967

Hamze-Ziabari, S. M., Razmi, A. M., Lemmin, U., & Barry, D. A. (2022). Detecting submesoscale cold filaments in a basin-scale gyre in large, deep Lake Geneva (Switzerland/France). *Geophysical Research Letters*, *49*(4), e2021GL096185. https://doi.org/10.1029/2021GL096185

Karimova, S. (2012). Spiral eddies in the Baltic, Black and Caspian seas as seen by satellite radar data. *Advances in Space Research*, *50*(8), 1107–1124. https://doi.org/10.1016/j.asr.2011.10.027

Kudryavtsev, V., Akimov, D., Johannessen, J., & Chapron, B. (2005). On radar imaging of current features: 1. Model and comparison with observations. *Journal of Geophysical Research*, *110*(C7), C07016. https://doi.org/10.1029/2004JC002505

Kujawinski, E. B., Farrington, J. W., & Moffett, J. W. (2002). Evidence for grazing-mediated production of dissolved surface-active material by marine protists. *Marine Chemistry*, *77*(2), 133–142. https://doi.org/10.1016/S0304-4203(01)00082-2

Kurata, N., Vella, K., Hamilton, B., Shivji, M., Soloviev, A., Matt, S., et al. (2016). Surfactant-associated bacteria in the near-surface layer of the ocean. *Scientific Reports*, *6*(1), 19123. https://doi.org/10.1038/srep19123

Lemmin, U., & D'Adamo, N. (1996). Summertime winds and direct cyclonic circulation: Observations from Lake Geneva. *Annales Geophysicae*, *14*(11), 1207–1220. https://doi.org/10.1007/s00585-996-1207-z

Liardon, J.-L., & Barry, D. A. (2017). Adaptable imaging package for remote vehicles. *HardwareX*, *2*, 1–12. https://doi.org/10.1016/j.ohx.2017.04.001

Mahadevan, A., & Tandon, A. (2006). An analysis of mechanisms for submesoscale vertical motion at ocean fronts. *Ocean Modelling*, *14*(3), 241–256. https://doi.org/10.1016/j.ocemod.2006.05.006

Marmorino, G. O., Askari, F., & Mied, R. (2002). Observations of the creation and evolution of small-scale oceanic frontal cusps and slicks. *Journal of Marine Systems*, *37*(1), 17–29. https://doi.org/10.1016/S0924-7963(02)00193-8

Marmorino, G. O., Smith, G. B., Toporkov, J. V., Sletten, M. A., Perkovic, D., & Frasier, S. J. (2008). Evolution of ocean slicks under a rising wind. *Journal of Geophysical Research*, *113*(C4), C04030. https://doi.org/10.1029/2007JC004538

McWilliams, J. C. (2016). Submesoscale currents in the ocean. *Proceedings of the Royal Society A: Mathematical, Physical & Engineering Sciences*, *472*(2189), 20160117. https://doi.org/10.1098/rspa.2016.0117

McWilliams, J. C. (2017). Submesoscale surface fronts and filaments: Secondary circulation, buoyancy flux, and frontogenesis. *Journal of Fluid Mechanics*, *823*, 391–432. https://doi.org/10.1017/jfm.2017.294

McWilliams, J. C. (2021). Oceanic frontogenesis. *Annual Review of Marine Science*, *13*(1), 227–253. https://doi.org/10.1146/annurev-marine-032320-120725

Naumenko, M. A., Guzivaty, V. V., & Karetnikov, S. G. (2012). Variability of the horizontal gradients of the air and the water surface temperatures in the vernal frontal zone period of Lake Ladoga. *Oceanology*, *52*(6), 735–740. https://doi.org/10.1134/S0001437012060082

O'Donnell, J., Marmorino, G. O., & Trump, C. L. (1998). Convergence and downwelling at a river plume front. *Journal of Physical Oceanography*, *28*(7), 1481–1495. https://doi.org/10.1175/1520-0485(1998)028<1481:CADAAR>2.0.CO;2

Phillips, O. M. (1984). On the response of short ocean wave components at a fixed wavenumber to ocean current variations. *Journal of Physical Oceanography*, *14*(9), 1425–1433. https://doi.org/10.1175/1520-0485(1984)014<1425:OTROSO>2.0.CO;2

Rahaghi, A. I., Lemmin, U., Sage, D., & Barry, D. A. (2019). Achieving high-resolution thermal imagery in low-contrast lake surface waters by aerial remote sensing and image registration. *Remote Sensing of Environment*, *221*, 773–783. https://doi.org/10.1016/j.rse.2018.12.018

Rascle, N., Chapron, B., Molemaker, J., Nouguier, F., Ocampo-Torres, F. J., Osuna Cañedo, J. P., et al. (2020). Monitoring intense oceanic fronts using sea surface roughness: Satellite, airplane, and in situ comparison. *Journal of Geophysical Research: Oceans*, *125*(8), e2019JC015704. https://doi.org/10.1029/2019JC015704

Rascle, N., Molemaker, J., Marié, L., Nouguier, F., Chapron, B., Lund, B., & Mouche, A. (2017). Intense deformation field at oceanic front inferred from directional sea surface roughness observations. *Geophysical Research Letters*, *44*(11), 5599–5608. https://doi.org/10.1002/2017GL073473

Razmi, A. M., Barry, D. A., Bouffard, D., Vennemann, T., Barry, C. E., & Lemmin, U. (2018). Currents of lake Geneva. In N. Chèvre, D. A. Barry, F. Bonvin, N. Graham, J.-L. Loizeau, H.-R. Pfeifer, et al. (Eds.), *Micropollutants in large lakes: From potential pollution to risk assessments* (pp. 141–172). EPFL Press. https://doi.org/10.1201/9781351240291

Reiss, R. S., Lemmin, U., Cimatoribus, A. A., & Barry, D. A. (2020). Wintertime coastal upwelling in Lake Geneva: An efficient transport process for deepwater renewal in a large, deep lake. *Journal of Geophysical Research: Oceans*, *125*(8), e2020JC016095. https://doi.org/10.1029/2020JC016095

Riffler, M., Lieberherr, G., & Wunderle, S. (2015). Lake surface water temperatures of European Alpine lakes (1989–2013) based on the advanced very high resolution radiometer (AVHRR) 1 km data set. *Earth System Science Data*, *7*(1), 1–17. https://doi.org/10.5194/essd-7-1-2015

Ryan, J. P., Fischer, A. M., Kudela, R. M., McManus, M. A., Myers, J. S., Paduan, J. D., et al. (2010). Recurrent frontal slicks of a coastal ocean upwelling shadow. *Journal of Geophysical Research*, *115*(C12), C12070. https://doi.org/10.1029/2010JC006398

Salter, M. E. (2010). *A role for natural surfactants in air-sea gas exchange? (Doctoral dissertation)*. University of Newcastle upon Tyne.

Shcherbina, A. Y., D'Asaro, E. A., Lee, C. M., Klymak, J. M., Molemaker, M. J., & McWilliams, J. C. (2013). Statistics of vertical vorticity, divergence, and strain in a developed submesoscale turbulence field. *Geophysical Research Letters*, *40*(17), 4706–4711. https://doi.org/10.1002/grl.50919

Wang, T., Barkan, R., McWilliams, J. C., & Molemaker, M. J. (2021). Structure of submesoscale fronts of the Mississippi River plume. *Journal of Physical Oceanography*, *51*(4), 1113–1131. https://doi.org/10.1175/JPO-D-20-0191.1

Watson, A. J., Bock, E. J., Jähne, B., Asher, W. E., Frew, N. M., Hasse, L., et al. (1997). Report Group 1—Physical processes in the microlayer and the air–sea exchange of trace gases. In P. S. Liss & R. A. Duce (Eds.), *The sea surface and global change* (pp. 1–34). Cambridge University Press. https://doi.org/10.1017/CBO9780511525025.002